

transported to the inner magnetosphere.

Injection of particles from the ionosphere is another possible source of plasma. Precipitation of energetic charged particles into the ionosphere forms secondary electrons that should have energies of 20 to 40 eV and, by electrostatically pulling out ions, could provide an alternative source for the warm population. Similar processes have been discussed for other planets (15). Photoelectrons also have energies of 20 to 40 eV and are another possible source of plasma.

The boundary implied by the "plasma edge" observations ( $L \approx 5$ ) can be interpreted in several ways. It may be the inner limit of magnetospheric convection due to residual effects of corotation associated with the small angle ( $\approx 7^\circ$ ) between Uranus' rotation axis and the solar wind (12) or to shielding by pressure gradient effects (16). The expected location of the convection limit in either case depends on presently unknown

parameters, such as the ionospheric conductivity, but an  $L$  value of about 5 is not implausible. Alternatively, the boundary may be ascribed to plasma absorption by Miranda and its location related to Miranda's minimum  $L$  value, although the consistency with observations of the absorption signatures (including the predicted precise location) expected from this mechanism remains among the unsettled questions.

#### REFERENCES AND NOTES

1. G. L. Siscoe, *Icarus* **24**, 311 (1975).
2. T. W. Hill, A. J. Dessler, M. E. Rassbach, *Planet. Space Sci.* **31**, 1187 (1983).
3. A. K. Ip and G.-H. Voigt, *J. Geophys. Res.* **90**, 6287 (1985).
4. D. E. Shemansky and G. R. Smith, *Geophys. Res. Lett.* **13**, 1 (1986).
5. S. A. Curtis, *Nature (London)* **318**, 47 (1985).
6. A. Eviatar and J. D. Richardson, *Astrophys. J. Lett.* **301**, L99 (1985).
7. H. S. Bridge *et al.*, *Space Sci. Rev.* **21**, 259 (1977).
8. N. F. Ness *et al.*, *Science* **233**, 85 (1986).
9. S. M. Krimigis *et al.*, *ibid.*, p. 97.
10. E. C. Stone *et al.*, *ibid.*, p. 93.
11. J. A. Slavin *et al.*, *J. Geophys. Res.* **90**, 6275 (1985).
12. V. M. Vasyliunas, *Geophys. Res. Lett.*, in press.
13. J. D. Richardson, A. Eviatar, G. L. Siscoe, *J. Geophys. Res.*, in press.
14. A. L. Broadfoot *et al.*, *Science* **233**, 74 (1986).
15. R. M. Thorne, *Geophys. Res. Lett.* **8**, 509 (1981).
16. G. L. Siscoe, *J. Geophys. Res.* **87**, 5124 (1982).
17. We are deeply indebted to the many organizations and individuals who made the Voyager 2 Uranus encounter an outstanding scientific event. We especially thank the entire Voyager project staff at NASA Headquarters and at the Jet Propulsion Laboratory for their support of this and other Voyager experiments. We owe special thanks to O. Divers, B. McDougal, N. Toy, R. Hungerford, and E. Miner for assistance with encounter planning and operations; to A. Bowes, P. Milligan, J. Quigley, and G. Gordon for general support and for data reduction and analysis; to W. Mish and his colleagues for extensive and creative support throughout the encounter; to F. Kuykendall, S. Philipson, and their colleagues for extensive and invaluable color displays of our data; to D. Balcom for technical assistance; to the SUN Microsystems University Donation Program, whose support made rapid data analysis and color spectrograms possible; and to SUN staff M. Thomas for technical support and M. Moran, M. Goldstein, S. Stein, and J. Ablak for arranging SUN's support. Supported by NASA under JPL Contract 953733.

31 March 1986; accepted 5 May 1986

## Energetic Charged Particles in the Uranian Magnetosphere

E. C. STONE, J. F. COOPER, A. C. CUMMINGS, F. B. McDONALD, J. H. TRAINOR, N. LAL, R. MCGUIRE,\* D. L. CHENETTE

During the encounter with Uranus, the cosmic ray system on Voyager 2 measured significant fluxes of energetic electrons and protons in the regions of the planet's magnetosphere where these particles could be stably trapped. The radial distribution of electrons with energies of megaelectron volts is strongly modulated by the sweeping effects of the three major inner satellites Miranda, Ariel, and Umbriel. The phase space density gradient of these electrons indicates that they are diffusing radially inward from a source in the outer magnetosphere or magnetotail. Differences in the energy spectra of protons having energies of approximately 1 to 8 megaelectron volts from two different directions indicate a strong dependence on pitch angle. From the locations of the absorption signatures observed in the electron flux, a centered dipole model for the magnetic field of Uranus with a tilt of 60.1 degrees has been derived, and a rotation period of the planet of 17.4 hours has also been calculated. This model provides independent confirmation of more precise determinations made by other Voyager experiments.

THE VOYAGER 2 ENCOUNTER WITH Uranus revealed a moderate-sized magnetosphere surrounding this giant planet. Because the nature (or even the presence) of this magnetosphere was unknown before the encounter, the cosmic ray system (CRS) (1) was cycled every 192 seconds between two configurations to provide observations over a wide range of possible intensities of trapped particles. The instrument functioned normally throughout the encounter.

The trajectories at Uranus of the spacecraft, the satellites Miranda, Ariel, Umbriel, Titania, and Oberon, and the  $\epsilon$  ring are shown in Fig. 1 in a magnetic coordinate

system based on the offset tilted dipole model of the Uranian planetary magnetic field (2). The spacecraft crossed the magnetic equator once near 1321 spacecraft event time and reached a minimum  $L$ -shell value of 4.6 at 1829 (3). Because of the  $60^\circ$  tilt of the dipole relative to the rotation axis, the satellites sweep across broad ranges of  $L$  values and magnetic latitude as the planet rotates.

*Electron spatial distributions.* The electron absorption signatures of the three major inner satellites are shown in Fig. 2; these data were obtained from single detector counting rates of three detectors in the CRS instrument (4). The electron energy thresh-

olds and detector geometric factors were estimated by analysis from the passive shielding surrounding each detector and from the energy deposit thresholds. The baseline counting rates of each detector were due to the interplanetary charged-particle background, primarily galactic cosmic rays. None of the counting rates displayed in Fig. 2 increased above background levels until Voyager 2 was well inside the magnetosphere. Rates from the highest electron energies rose above background only inside the orbit of Miranda. Although the spacecraft reached an  $L$ -shell value of only 4.6, the rapid increase in the intensity of high-energy electrons ( $\approx 7.6$  MeV, curve 2 in Fig. 2) indicates an intense, high-energy radiation environment inside the region probed by Voyager 2.

At much lower electron energies, there are large spatial gradients in the magnetospheric flux in the outer magnetosphere (curve 1 in Fig. 3). Analysis of electronic pulse height data from the encounter and from calibrations after Voyager 2 was launched shows that this counting rate is dominated by the pile-up of low-energy ( $\approx 20$  keV) electrons.

E. C. Stone, J. F. Cooper, A. C. Cummings, George W. Downs Laboratory of Physics, California Institute of Technology, Pasadena, CA 91125.  
F. B. McDonald, NASA Headquarters, Washington, DC 20546.  
J. H. Trainor, N. Lal, R. McGuire, Goddard Space Flight Center, Greenbelt, MD 20771.  
D. L. Chenette, Aerospace Corporation, Los Angeles, CA 90009.

\*Concurrent affiliation: Department of Physics and Astronomy, University of Maryland, College Park, MD 20742.

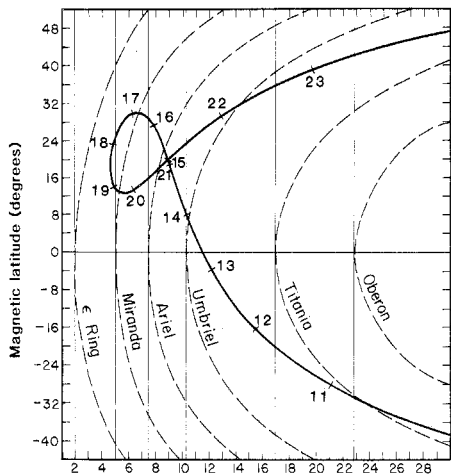


Fig. 1. Magnetic latitude versus dipole  $L$  for the Voyager 2 spacecraft, the five major inner satellites of Uranus, and the  $\epsilon$  ring. The hourly time tick marks along the Voyager 2 trajectory are in spacecraft event time. The vertical lines mark the minimum  $L$  value reached by each satellite and the  $\epsilon$  ring.

The spatial gradients suggest a stable trapping region extending out to  $L = 18$  to  $20$  in the dayside magnetosphere. On the nightside, this rate drops sharply at  $L \sim 17$ , which is consistent with the location of the hinge point of the magnetotail current sheet at about 18 Uranus radii ( $R_U$ ) (2).

The electron fluxes in Fig. 2 show pairs of significant satellite absorption signatures superimposed on a general increase in intensity with decreasing distance from Uranus. Each signature is broad and was observed on the inbound and the outbound passes of the spacecraft near the minimum  $L$  shell of each satellite. Because the satellites were not typically near their minimum  $L$  shells when the features were observed, this suggests that they are long-lived, stable characteristics of the electron flux distribution. It is clear from Fig. 2, therefore, that Umbriel, Ariel, and Miranda play a major role in limiting the overall intensity of the electron flux within the Uranian magnetosphere.

With the exception of a small feature in the counting rate for electrons above 1.1 MeV at 1445 spacecraft event time (during a roll maneuver), every minimum in the electron flux correlated with the minimum  $L$ -shell location of one of the known satellites of Uranus. We found no evidence in these electron counting rates for any "fresh" small-scale signatures resulting from recent absorption by any satellite or other material. No decrease in electron flux was observed in association with Titania, and Oberon is outside the region where significant fluxes of electrons above 1.1 MeV were observed.

In Fig. 2 we also show for comparison the electron counting rate profile observed

above 1.1 MeV along the Voyager 2 passage through the magnetosphere of Saturn. The Saturn data are plotted such that the  $L$  shell of each observation is the same for both the Saturn and the Uranus data sets as a function of time along the Voyager 2 Uranus encounter trajectory. The shape of the spacecraft trajectory in magnetic latitude versus  $L$  was not the same at Uranus as at Saturn. These differences in the latitude of the spacecraft as a function of  $L$ , and also between the inbound and outbound portions of each trajectory, must be taken into account in any detailed comparison of these data. Nevertheless, this comparison makes clear the importance of satellite absorption on the spatial distribution of the electron flux at Uranus. In contrast, the effects of the Saturnian satellites Rhea ( $L = 8.8$ ) and Dione ( $L = 6.3$ ) are not so apparent. At Saturn the rate of absorption of approximately 1-MeV electrons by the satellites was small because the longitudinal drift velocity of these electrons was comparable to the satellite's orbital velocity (5). At Uranus the relative drift velocities are an order of magnitude higher than at Saturn, leading to increased absorption.

The flux maximum near  $L = 6$ , between the orbits of Miranda and Ariel, shows a large inbound-outbound asymmetry that may indicate a steep pitch angle distribution. While inbound through this region Voyager 2 was at a magnetic latitude of  $+29^\circ$ , and while outbound the spacecraft was at  $+13^\circ$  (Fig. 1). An electron flux pitch angle ( $\alpha$ ) distribution of the form  $\sin^{2n}(\alpha)$  (where  $n$  is the pitch angle index) could account for the magnitude of the effect observed in the counting rate for electrons above 1.1 MeV if  $n$  were  $1.6 \pm 0.8$ . For the energy range greater than 3.1 MeV, the required  $n$  is  $3.5 \pm 0.8$ .

These estimates are initial and do not take into account the effects of the detectors' view direction relative to the pitch angle distribution; they assume that the detector response is isotropic. Also, the inbound and outbound positions of Voyager 2 with respect to the orbit of Miranda (dashed curve in Fig. 1) could have an effect on these results. On the outbound pass at  $L = 6$ , a significant fraction of the measured electrons could not have crossed Miranda's magnetic latitude and had no probability of absorption, whereas all particles measured

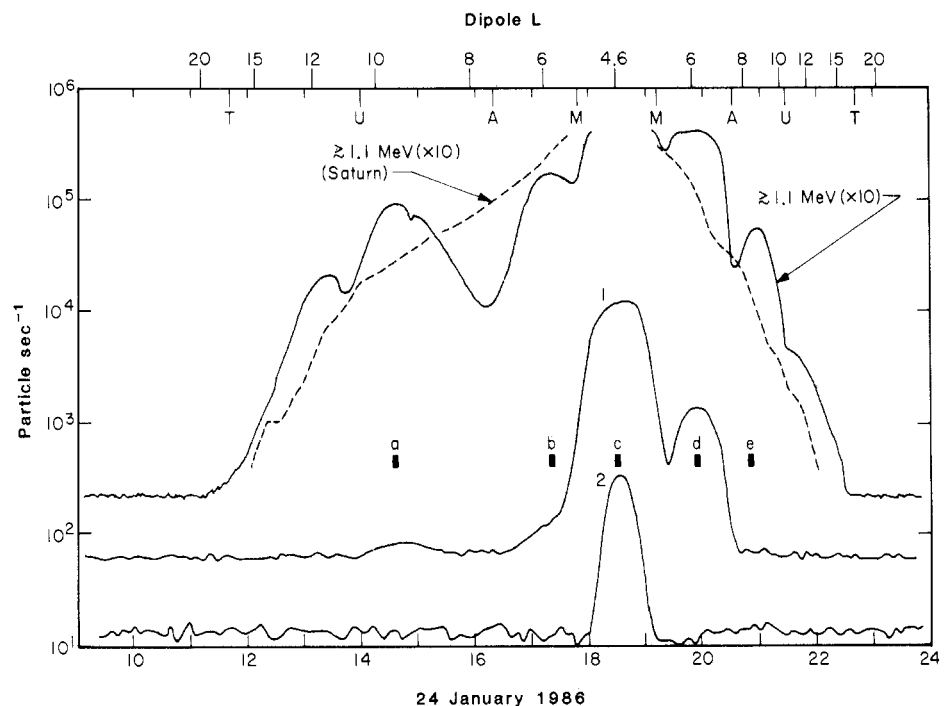


Fig. 2. Voyager 2 electron counting rates (4). Curves 1 and 2 display rates for energies greater than 3.1 and 7.6 MeV, respectively. The rate for electrons greater than 1.1 MeV is multiplied by a factor of 10 for clarity. Data gaps, due to instrument cycling and incomplete initial data sets, are filled in by interpolation. The  $L$  coordinates on the upper scale were calculated on the assumption of an offset tilted dipole model of the magnetic field (2). The dashed curve is the electron counting rate for the 1.1-MeV energy threshold ( $\times 10$ ) at Saturn, plotted as a function of the  $L$  coordinate. The rates shown are not corrected for dead-time effects, and data near  $L = 5$  for the lowest energy rates have been deleted because of saturation effects. In addition, the counting rate above 1.1 MeV was high enough around 2000 spacecraft event time that the true counting rate is significantly higher than that plotted. The vertical ticks labeled T, U, A, and M mark the minimum  $L$  values of the satellites Titania, Umbriel, Ariel, and Miranda, respectively. The bars labeled a through e mark periods during which the electron spectra in Fig. 4 were obtained.

inbound at  $L = 6$  had to cross Miranda's orbit to reach Voyager 2.

**Protons.** Several CRS proton counting rates are shown in Fig. 3. The fluxes for 3.2- to 5-MeV protons are derived from three-parameter pulse height analysis. They provide clear evidence for stable trapping of megaelectron volt-protons inside  $L \sim 10$ , with flux levels at least 100 times those measured just before Voyager 2 entered the magnetosphere. These proton fluxes are comparable to those measured in the outer magnetosphere of Saturn (6) above the same energy thresholds. The relative variations of the proton fluxes measured from two low-energy telescopes at right angles to one another (for example, at 1400 to 1730 spacecraft event time) are presumably due to anisotropies in pitch angle distributions.

For galactic cosmic rays the fourfold coincidence rate in Fig. 3 (curve 3) responds primarily to protons at energies of 63 to 160 MeV and to helium nuclei at energies greater than 70 MeV per nucleon; the latter dominates the nominal response. At Saturn this rate indicated a significant flux of high-energy protons in the inner magnetosphere from cosmic ray albedo neutron decay (CRAND) (6, 7). At Uranus, however, there is a decrease rather than an increase inside  $L \sim 5$ . This decrease by a factor of 2 at 1800 to 1900 spacecraft event time is consistent with the predicted energy cutoffs for cosmic ray nuclei, corresponding to the vertical Störmer cutoff in magnetic rigidity (that is, momentum over charge) of  $42/L^2$  GV based on a magnetic dipole moment of about  $0.23 \text{ G R}_U^3$  (2). The minimum  $L$  of 4.6 during the encounter corresponds to kinetic energy cutoffs of 1.3 and 0.4 GeV per nucleon for protons and heavier nuclei ( $A/Z \approx 2$ ), respectively.

An estimate for the stable trapping limit is one-sixth the vertical Störmer cutoff rigidity (8), or  $7.0/L^2$  GV for Uranus. Thus the absence of CRAND protons with energies greater than 63 MeV at  $L = 4.6$  is expected because the stable trapping limit corresponds to about 60 MeV. However, 3-MeV protons can be stably trapped at  $L \leq 10$ , which is consistent with the increased low-energy fluxes shown in Fig. 3.

In Fig. 4A we show the differential energy spectrum of protons from three identical low-energy telescopes (LET's) of the CRS instrument for the time period 1530 to 1630 spacecraft event time. At energies less than about 1.8 MeV, the data are from LET A, which was configured so that energy deposits in the front 35- $\mu\text{m}$  detector could be measured. These data join smoothly to the higher energy data from LET C, which was configured so that a coincidence between the first two detectors (both 35  $\mu\text{m}$

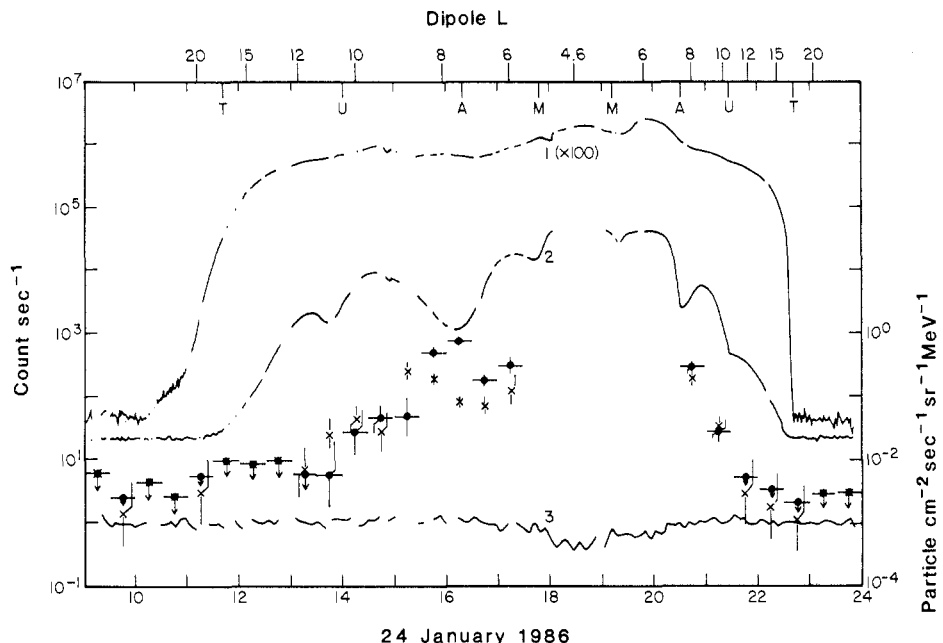


Fig. 3. Counting rates and proton fluxes at Uranus (4). Curve 1 is the rate ( $\times 100$ ) from a 35- $\mu\text{m}$  detector with a 0.2-MeV threshold shielded by a 3- $\mu\text{m}$  aluminum foil. It responds to protons with energies greater than 0.43 MeV and to pileup of low-energy electrons ( $\geq 20$  keV). Curve 2 is from Fig. 2 and represents the electron rate above 1.1 MeV. Curve 3 represents a fourfold coincidence rate corresponding to protons with energies from 63 to 160 MeV and to helium nuclei with energies greater than 70 MeV per nucleon. The data points represent fluxes of 3.2- to 5-MeV protons as measured with LET C ( $\bullet$ ) and LET D ( $\times$ ) (1). From 1730 to 2030 spacecraft event time, the flux of 3.2- to 5-MeV protons is not available. The  $L$  coordinates and satellite positions are from Fig. 2.

thick) was required for pulse height analysis. LET A and LET C have a  $50^\circ$  field of view in opposite directions, so that they sample the same pitch angles.

During the period when these spectra were accumulated, Voyager 2 traveled from  $L = 8.5$  to 7.2, with associated trapping limits ranging in rigidity from about 97 to 135 MV. For protons, the corresponding maximum energies for stable trapping varied from about 5 to 10 MeV. For helium and other nuclei with  $A/Z = 2$ , the corresponding maximum energies ranged from about 1 to 2 MeV per nucleon. Thus fluxes of stably trapped heavy nuclei with energies of 3.2 to 5 MeV per nucleon would not have been expected in this region. The one helium nucleus in this energy interval that was observed during this period was probably not part of the trapped population.

At energies ( $E$ ) less than about 2.5 MeV, the proton spectrum from LET A and LET C in Fig. 4 was consistent with  $j \propto E^{-2.8}$ , but at higher energies the spectrum steepened sharply to  $j \propto E^{-8.5}$  ( $j$ , directional flux). The spectrum from LET D, which points  $90^\circ$  away from the view directions of LET A and LET C, was substantially lower in intensity than the LET C spectrum (Fig. 4). This difference approached a factor of 10 at about 1.8 MeV and was apparently due to the pitch angle dependence of the proton intensity.

**Electron spectra and sources.** Figure 4B shows estimates for integral electron spectra at the five times shown in Fig. 2 (marked a to e). These times correspond approximately to maxima in the electron rates, which occurred between the minimum  $L$ -shell positions of the large Uranian inner satellites. Inside the minimum  $L$  shell of Miranda, the spectrum could be measured to the highest energies ( $\geq 10.3$  MeV). At this time the spectrum above about 3 MeV was steep ( $J \propto E^{-15}$ ), whereas below 3 MeV it was much flatter ( $J \propto E^{-4}$ ).

The spectra in Fig. 4 were used to make initial estimates of the radial dependence of the electron phase space density (9):

$$f(M, L, \alpha = 90^\circ) = \frac{v J_{\perp}(E, L)}{p^2(M, L) E(M, L)} \quad (1)$$

where  $p(M, L)$  and  $E(M, L)$  (the electron momentum and kinetic energy, respectively) are functions of  $L$  and the first magnetic invariant,  $M = p^2/2mB_0$ ; the equatorial magnetic field is  $B_0 = 0.23/L^3$  G (2);  $m$  is the electron rest mass;  $J_{\perp}$  is the directional flux perpendicular to the magnetic field line at the equatorial plane; and  $v$  is the power-law index for an integral flux  $J_{\perp}(E, L) \propto E^{-v}$  of equatorially trapped particles. The equatorial flux is estimated from  $J_{\perp} \approx J(E, L)(B/B_0)^n$  in terms of the local measured integral flux  $J(E, L)$ , the local magnetic field  $B$ , and the index  $n$  for the pitch

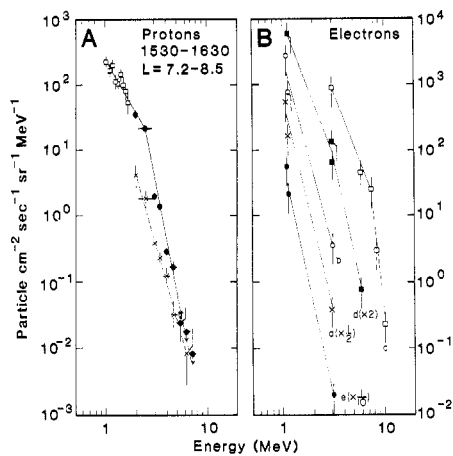


Fig. 4. (A) Differential energy spectra of protons and (B) estimated integral spectra of electrons in the magnetosphere of Uranus. The proton spectra are for the period 1530 to 1630 spacecraft event time. Data from LET A ( $\square$ ), LET C ( $\bullet$ ), and LET D ( $\times$ ) ( $L$ ) are shown. The electron spectra are for five 6.4-minute periods labeled a to e in Fig. 2. The spacecraft event times ( $T$ ) and positions of these spectra are as follows: a,  $T = 1435$ ,  $L = 9.6$ ; b,  $T = 1722$ ,  $L = 5.7$ ; c,  $T = 1832$ ,  $L = 4.6$ ; d,  $T = 1955$ ,  $L = 6.2$ ; and e,  $T = 2053$ ,  $L = 8.4$ . For clarity, the intensities in periods a, d, and e are multiplied by the factors shown.

angle distribution  $J(\alpha) \propto \sin^{2n}\alpha$  (where  $n$  is approximately 1.6 to 3.5 as previously estimated at  $L = 6$ ). This estimate assumes omnidirectional response of the electron detectors due to their wide fields of view. The relative phase space densities are shown in Table 1 for electrons with pitch angle indices of 1.5 and 3.0 and for  $M$  values of 8,000  $\text{MeV G}^{-1}$  and 15,000  $\text{MeV G}^{-1}$ , which correspond to electron energies within the range of the measured spectra in Fig. 4B. Taking into consideration the directional response by the electron detectors may introduce corrections to these estimates.

Although further studies are required to characterize the radial diffusion and satellite absorption processes, the positive radial gradients evident for the phase space densities in Table 1 indicate radially inward diffusion and acceleration at  $L > 6$ . The solar wind could not be the direct source, however, because the electrons above 1.1 MeV at  $L = 9.6$  with  $M$  greater than 8700  $\text{MeV G}^{-1}$  would have energies greater than 0.4 MeV at the subsolar magnetopause, where  $B$  is approximately  $6 \times 10^{-5}$  G (2). Even the lowest energy electrons observed at 1722 spacecraft event time and  $L \sim 5.7$  with  $M$  values of about 1900  $\text{MeV G}^{-1}$  would require a 100-keV source if located near the subsolar magnetopause. Curve 1 in Fig. 3 is consistent with a large flux of 10- to 100-keV electrons in the outer magnetosphere. Possible sources include the magnetotail or

Table 1. Estimated electron phase space densities (relative units).

Spacecraft event time	$L$	Magnetic latitude (degrees)	Phase space density			
			$M = 8,000 \text{ MeV G}^{-1}$		$M = 15,000 \text{ MeV G}^{-1}$	
			$n = 1.5$	$n = 3.0$	$n = 1.5$	$n = 3.0$
1435	9.6	+14	3,800	5,700	99	150
2053	8.4	+19	300	600	6.3	13
1955	6.2	+13	42	59	4.6	6.6

nonadiabatic processes induced by the oblique rotation of the magnetic dipole.

**Absorption signature magnetic field models.** By absorbing charged particles, the satellites within the magnetosphere of Uranus provide a way to measure the shape of the magnetic field. Because charged particles closely follow magnetic field lines in the course of their latitudinal bounce motion, absorption signatures identify field lines at latitudes far from the satellite orbit plane. Also, because charged particles drift in longitude around the magnetic axis, the long-lived, stable absorption signatures identify drift shells of field lines at given values of  $L$ . Thus, absorption signatures from the same satellite observed at different locations in the magnetosphere provide a large-scale measure of the geometry of the magnetic field that is complementary to the local vector measurements obtained by the magnetometer along Voyager 2's trajectory.

We observed a pair of absorption signatures from the three major inner satellites Umbriel, Ariel, and Miranda (each pair along the inbound and outbound passes). We used these features to derive the centered dipole magnetic field model that provides the best fit to the observed positions of the signatures and to determine the rotation rate of the internal source of the field. The model was restricted to a centered dipole

because that is the lowest order part of any magnetic field model and because only three observations were available to be fit.

The position of the flux minimum for electrons above 1.1 MeV that corresponded to each absorption signature and the uncertainty in that position were calculated from the predicted spacecraft trajectory and the times and timing uncertainties associated with each observation. Using a dipole centered on Uranus, we converted the positions and uncertainties of the features to magnetic dipole  $L$ . The optimum dipole field model was determined by varying the tilt angle, tilt direction, and rotation period to minimize the quantity

$$G = \sum \frac{(L_i - L_o)^2}{(\sigma_{L_i})^2 + (\sigma_{L_o})^2} \quad (2)$$

where the sum is over the three pairs of signatures observed inbound ( $i$ ) and outbound ( $o$ ).  $G$  is the "goodness-of-fit" of the model to the data and is defined by analogy with the standard definition of the statistical parameter  $\chi^2$ .

The results of this study are summarized in Fig. 5, where we plot the value of  $G$  as a function of each of the three parameters in the vicinity of the minimum. With the rotation period fixed at 17.3 hours, the best-fit values for the dipole tilt angle and direction were  $60.1^\circ$  tilt toward  $+229^\circ$  longitude

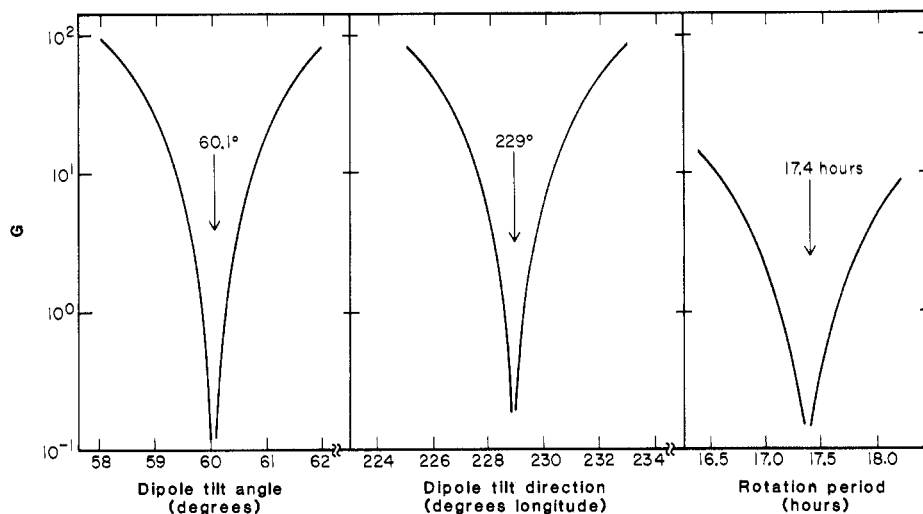


Fig. 5. Goodness of fit ( $G$ ) for three parameters of a Uranian magnetic field model as determined from absorption features in the counting rate for electrons above 1.1 MeV.

Table 2. Positions of flux minima for electron energies greater than 1.1 MeV compared to positions of satellite  $L$  shells.

Satellite Name	Minimum $L$ shell	Position of minimum		
		Centered dipole $L$	Offset dipole $L$	
			In- bound	Out- bound
Miranda	5.0	5.6	5.2	5.2
Ariel	7.4	7.9	7.6	7.6
Umbriel	10.3	10.6	10.8	10.2

(10). When the rotation period was also allowed to vary, the best-fit period obtained was 17.4 hours, and with the 17.4-hour period, the best-fit orientation of the dipole was the same to within  $0.1^\circ$  in both tilt angle and direction. Because we have only three feature pairs to use in the model fit, the assignment of formal uncertainties is difficult. However, as illustrated in Fig. 5, the best-fit values of both the tilt angle and the tilt direction are well determined (probably to better than  $0.5^\circ$  and  $1^\circ$ , respectively), and the rotation period is determined to better than 0.5 hour.

The tilt angle, tilt direction longitude, and rotation rate were determined independent of the results obtained by Ness (2) and Warwick (11) and their colleagues from their analysis of Voyager 2 data. The parameters of the resulting models are in good agreement, even though the magnetometer model also includes an offset from the center of Uranus. Our analysis provides an independent measurement of the large tilt angle and direction of the lowest order (dipole) term as well as of the rotation period of the planetary interior.

The large angle between the magnetic dipole and rotation axes causes each satellite to sweep out a wide range in  $L$  during each half-rotation of Uranus (Fig. 1). Absorption of charged particles, however, is most effective near the minimum  $L$  shell of each satellite. There are two reasons for this effect: (i) each satellite spends most of its time in the band of  $L$  shells near its minimum, and (ii) when a satellite is not near its minimum  $L$  shell, it is at higher latitudes and cannot absorb particles that mirror at smaller magnetic latitudes. Thus the minima in the particle absorption signatures are expected to occur near the minimum  $L$  shell of each satellite.

As illustrated in Table 2, however, the  $L$  shells where absorption signature minima were observed were generally outside these expected locations. With the centered dipole model, these deviations were 0.3 to 0.6 in  $L$ , increasing toward smaller values of  $L$ ; with

the offset dipole model (2), the deviations were significantly smaller (0.2 in  $L$ ), except at Umbriel. These results suggest that high-order moments of the field are important to the field geometry.

As shown in Table 2, the offset dipole model does not accurately describe the electron drift shell at Umbriel, perhaps because Umbriel is at a distance from Uranus where external contributions to the field are important. The inbound-outbound asymmetry in the position of Umbriel's signature is in the same direction as the drift shell asymmetry expected from dayside compression of the magnetosphere. Further analysis of these results will lead to better values of the internal and external components of the magnetic field at Uranus.

#### REFERENCES AND NOTES

- For a description of the CRS system on Voyagers 1 and 2, see E. C. Stone *et al.*, *Space Sci. Rev.* **21**, 355 (1977).
- N. F. Ness *et al.*, *Science* **233**, 85 (1986).
- We define  $L$  as  $R/\cos^2(\lambda)$ , where  $R$  is the radial distance from the center of the offset magnetic dipole in Uranus radii ( $1 R_U = 25,600$  km) and  $\lambda$  is the magnetic latitude. The rotational pole currently illuminated by the sun is the southern (negative latitude) pole, as defined by the International Astronomical Union.
- Counting rates were obtained from the following detectors of the CRS instrument: D1 ( $\approx 1.1$ -MeV electrons),  $G \sim 11$  cm<sup>2</sup> sr, 100% duty cycle; C4 (high gain,  $\approx 3.1$ -MeV electrons),  $G \sim 20$  cm<sup>2</sup> sr, 3% duty cycle; C4 (low gain,  $\approx 7.6$ -MeV electrons),  $G \sim 13$  cm<sup>2</sup> sr, 3% duty cycle; L1 (no gain change,  $\approx 0.43$ -MeV protons and pile-up of  $\approx 20$ -keV electrons),  $G \sim 4.5$  cm<sup>2</sup> sr, 100% duty cycle (Fig. 3, curve 1); B2, C4, C3, and C2 (coincidence, low gain, 63- and 160-MeV protons and  $\approx 70$ -MeV helium),  $G \sim 11$  cm<sup>2</sup> sr, 50% duty cycle (Fig. 3, curve 3) [see (1) for more information].
- J. A. Van Allen *et al.*, *J. Geophys. Res.* **85**, 5709 (1980).
- R. E. Vogt *et al.*, *Science* **215**, 577 (1982).
- A. W. Schardt and F. B. McDonald, *J. Geophys. Res.* **88**, 8923 (1983).
- J. R. Thomas and W. R. Doherty, *JPL Tech. Mem.* 33-543 (1972), p. 315.
- M. Schulz and L. J. Lanzerotti, *Particle Diffusion in the Radiation Belts*, (Springer-Verlag, New York, 1974).
- The longitude system used here is that recommended by the Voyager Project Office, in which the longitude of Voyager 2 at 1800 spacecraft event time on 24 January 1986 was  $+121^\circ$  (where positive longitudes are measured clockwise as viewed from above the rotation pole currently illuminated by the sun).
- J. W. Warwick *et al.*, *Science* **233**, 102 (1986).
- We thank R. E. Vogt for his contributions during his tenure as principal investigator for the CRS system on Voyager 2; we are also indebted to the late A. W. Schardt, whose contributions to the analysis of the CRS data at Jupiter and Saturn were an important factor in our understanding of the Uranian magnetosphere. We thank the Voyager project members and the enthusiastic staff of our laboratories at Caltech and Goddard Space Flight Center for their excellent support; special thanks go to P. Schuster, T. Garrard, R. Burrell, L. Thomas, and O. Divers. Supported by NASA under contracts NAS7-918 and NGR 05-002-160. D.L.C. was supported in part by the Aerospace Corporation's sponsored research program.

31 March 1986; accepted 5 May 1986

## The Magnetosphere of Uranus: Hot Plasma and Radiation Environment

S. M. KRIMIGIS, T. P. ARMSTRONG, W. I. AXFORD, A. F. CHENG, G. GLOECKLER, D. C. HAMILTON, E. P. KEATH, L. J. LANZEROTTI, B. H. MAUK

The low-energy charged-particle (LECP) instrument on Voyager 2 measured low-energy electrons and ions near and within the magnetosphere of Uranus. Initial analysis of the LECP measurements has revealed the following. (i) The magnetospheric particle population consists principally of protons and electrons having energies to at least 4 and 1.2 megaelectron volts, respectively, with electron intensities substantially exceeding proton intensities at a given energy. (ii) The intensity profile for both particle species shows evidence that the particles were swept by planetary satellites out to at least the orbit of Titania. (iii) The ion and electron spectra may be described by a Maxwellian core at low energies (less than about 200 kiloelectron volts) and a power law at high energies (greater than about 590 kiloelectron volts; exponent  $\gamma$ , 3 to 10) except inside the orbit of Miranda, where power-law spectra ( $\gamma$  approximately 1.1 and 3.1 for electrons and protons, respectively) are observed. (iv) At ion energies between 0.6 and 1 megaelectron volt per nucleon, the composition is dominated by protons with a minor fraction (about  $10^{-3}$ ) of molecular hydrogen; the lower limit for the ratio of hydrogen to helium is greater than  $10^4$ . (v) The proton population is sufficiently intense that fluences greater than  $10^{16}$  per square centimeter can accumulate in  $10^4$  to  $10^5$  years; such fluences are sufficient to polymerize carbon monoxide and methane ice surfaces. The overall morphology of Uranus' magnetosphere resembles that of Jupiter, as evidenced by the fact that the spacecraft crossed the plasma sheet through the dawn magnetosheath twice per planetary rotation period (17.3 hours). Uranus' magnetosphere differs from that of Jupiter and of Saturn in that the plasma  $\beta$  is at most 0.1 rather than 1. Therefore, little distortion of the field is expected from particle loading at distances less than about 15 Uranus radii.